INTERACTIVE PROGRAMMING OF FILAMENT WINDING OPERATIONS ON CNC MACHINES

Oleh Kivirenko [0000-0001-7729-2337], Vladyslav Voronko [0000-0003-1020-0412], Illia Vasyliev [0009-0009-1260-0656], Serhii Terzin [0009-0003-1398-6649], Stanislav Kostenko [0000-0003-0268-8008], Iaroslav Dolzhenko [0009-0008-9657-7336], Yevgen Tsegelnyk [0000-0003-1261-9890]
School of Energy, Information and Transport Infrastructure, O.M. Beketov National University of Urban Economy in Kharkiv, 17 Chornohlazivska Street, Kharkiv 61002, Ukraine
E-mail: y.tsegelnyk@kname.edu.ua (✉)

Abstract – Filament winding is a widely used manufacturing technology for producing fiber-reinforced polymer (FRP) pipes and tubular structures with tailored mechanical properties. The quality and repeatability of the winding process strongly depend on the accuracy of trajectory generation, smooth motion control, and correct coordination of machine axes, especially when using low-cost CNC winding machines with a limited number of controlled axes. This paper presents an approach to interactive programming of filament winding operations directly on CNC machines, without the use of external CAM systems. Mathematical models for helical and circumferential winding layers, as well as transition trajectories between layers, are developed for a two-axis winding scheme. The proposed models ensure uniform fiber distribution, controlled overlapping, and smooth motion in reversal zones by applying circular interpolation instead of conventional linear interpolation. An approach to the development of a dedicated software application is presented, and an interactive tool integrated into the CNC programming environment is described. The application enables layer-by-layer design of winding structures, automatic calculation of winding parameters, and direct generation of CNC programs. Experimental validation based on quantitative wall thickness measurements was carried out on a two-axis winding machine during the manufacture of glass-fiber composite pipes. The results demonstrate stable winding patterns, uniform wall thickness, and reliable reproducibility of the programmed trajectories, confirming the practical applicability of the proposed interactive CNC-based programming approach.

Keywords: Filament winding, CNC programming, Interactive process design, Winding trajectory generation, FRP pipes, Helical winding, Circumferential winding, Low-cost CNC machines.

1. Introduction

The development of pipe materials has been a continuous process driven by technological advances, changing industrial needs, and a growing understanding of material properties. Over time, various materials have been used to manufacture pipes, each with its own advantages and disadvantages. At the current stage of industrial development, technologies for manufacturing pipelines from fiber-reinforced polymer (FRP) materials are considered particularly promising [1–3]. The most promising industries for the application of FRP pipelines include the oil and gas industry, civil engineering, aviation, shipbuilding (marine construction), and cryogenic engineering [1, 4, 5].

Various technologies are used to produce fiber-reinforced pipes. For example, fiberglass pipeline continuous filament winding [3] enables the manufacture of pipes with virtually unlimited length; however, it is based on cross-ply longitudinal–transverse winding. A major drawback of this approach is the use of non-impregnated fibers for forming longitudinal reinforcement. In contrast, in helical filament winding technologies all reinforcing fibers are impregnated during the winding process [6–8].

It should be noted that in helical winding of both cylindrical pipelines and complex-shaped components such as pressure vessels, each layer is always formed through multiple passes. Variations in the sequence of these passes result in different

dx.doi.org/10.17683/ijomam/issue23.31

winding patterns, whose influence on the technological and structural characteristics of FRP products has been actively investigated using CAE tools and experimental studies [6, 7].

The manufacturing process of FRP pipelines involves the sequential winding of fibers onto a cylindrical mandrel. The orientation of the fibers and the uniformity of their distribution within the pipe wall strongly determine the physical and mechanical properties of the final product [4, 6, 9]. This process is performed on CNC equipment and requires appropriate mathematical models and software for calculating winding trajectories [7, 10].

The accuracy of the equipment and the stability of process parameter reproduction are critical factors affecting both the quality and mechanical performance of the formed pipe wall material. The influence of fiber winding speed on the mandrel has been experimentally confirmed in previous studies [11]. The effect of winding structure is commonly assessed through the quality of the winding pattern. It has been shown that winding pattern quality depends not only on the winding angle, but also on the controllability of reversal zones, kinematic accuracy, and stability of contact conditions during the winding process [8]. Several approaches to trajectory generation and winding pattern planning for filament winding machines have been proposed in the literature, including analytical models, simulation-based optimization, and CAM-based trajectory generation methods [7, 12, 13]. However, in practical implementations, winding trajectories are often programmed using linear interpolation segments, which are characterized by non-smooth variations of differential motion characteristics such as velocity and acceleration. This negatively affects motion stability in reversal zones and reduces process reliability [14, 15]. Recent studies demonstrate active development of advanced winding technologies and related manufacturing approaches aimed at improving process stability, material structure, and functional properties of tubular products. In [16], a method for winding small-diameter pipes using vibration effects is proposed, showing that controlled external dynamic influences can significantly affect fiber placement quality and structural uniformity of composite pipes. This highlights the importance of precise trajectory control and stable motion behavior during winding, especially for pipes with small diameters and strict geometric tolerances.

Broader trends in advanced manufacturing also emphasize the growing role of digitally driven and hybrid production technologies. In [17], a comprehensive review of metal additive manufacturing processes is presented, underlining the importance of process planning, trajectory generation, and control strategies in achieving predictable material properties. Although focused on additive manufacturing, these methodological approaches are conceptually relevant to filament winding, particularly in the context of CNC-based trajectory generation without reliance on external CAM systems.

Energy-assisted manufacturing processes further illustrate the importance of controlled technological conditions. In [18], the authors investigated the use of microwave energy for adsorbent regeneration, demonstrating how regulated energy input affects internal material processes and system efficiency. While addressing a different application domain, this work emphasizes the broader significance of process controllability and stable parameter regulation, which are likewise critical for filament winding operations.

In addition, advances in the design and control of special-purpose electromechanical systems support the development of application-oriented CNC equipment. In [19] proposed object-oriented design principles for special-purpose induction electrical machines, illustrating how tailored electromechanical solutions can enhance the performance and controllability of complex engineering systems. These concepts are directly applicable to low-cost winding machines, where machine kinematics and control architecture must be closely aligned with the programmed technological process.

Despite the widespread industrial application of filament winding technologies, research aimed at improving machine kinematics and control systems for filament winding remains highly relevant [10, 20, 21]. A key aspect of ensuring high-quality winding of tubular structural elements is the uniform filling of the pipe wall volume with reinforcing fibers, without gaps or overlaps [22]. This requirement is ensured by both the correctness of winding trajectory calculation [7, 10] and the accuracy of actuator control in CNC equipment [14, 23].

In this paper, an approach focused on the development of a simple and practical method for generating filament winding trajectories for cylindrical pipelines on low-cost two-axis CNC winding machines is presented. A distinctive feature of the proposed trajectories is the use of circular interpolation to ensure smooth variation of mandrel rotational speed and delivery head motion in reversal zones. The objective of this study is to develop a methodology for calculating and programming filament winding trajectories directly on two-axis CNC winding equipment.

2. Materials and Methods

2.1 Research Methodology

The study presented in this paper was carried out in accordance with the research scheme shown in Figure 1. The methodology includes an analysis of the filament winding process for fiber-reinforced polymer pipelines, as well as the development of mathematical models and software integrated into the CNC system of a low-cost two-axis winding machine.

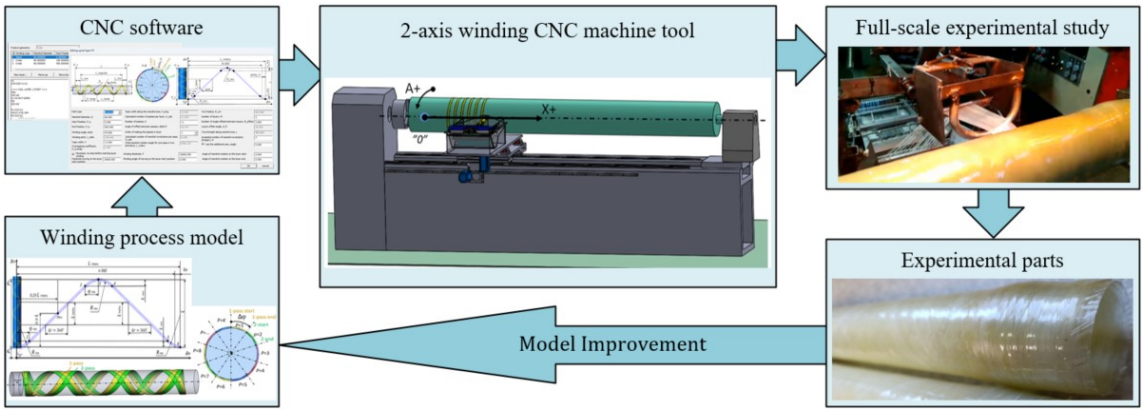

Figure 1: Scheme for conducting experimental studies

Experimental validation of the proposed approach was performed through full-scale tests on a two-axis winding machine. Deviations in the wall thickness of the manufactured pipe specimens were used as an indicator of the uniformity of reinforcing fiber placement.

In this section, the general technological scheme for pipe manufacturing by filament winding on a rigid mandrel is considered. The main types of winding layers used in pipe production are analyzed, and the layer types applicable to two-axis winding equipment are selected. Mathematical models for calculating the winding trajectories of helical and circumferential layers are developed. For helical winding, it is proposed to perform motion reversal zones of the delivery head along trajectories defined by circular interpolation, in contrast to the conventional approach based on linear interpolation of trajectories.

Section 3 presents a contextual model of the winding process that defines the principles for developing software for interactive programming of winding operations on CNC equipment. The results of developing software integrated into the CNC system of a low-cost two-axis winding machine are described. Examples of generating CNC programs for helical and circumferential winding layers used in the fabrication of experimental pipe specimens are provided. Section 4 describes the procedure for conducting full-scale experimental studies on a two-axis winding machine and presents the results of evaluating fiber winding uniformity based on measured deviations in pipe wall thickness.

2.2 Types of Winding Layers in Pipe Manufacturing

A wide range of technologies are used for the manufacture of fiber-reinforced polymer pipes. These include prepreg winding, winding of dry reinforcing material followed by pultrusion impregnation, and the most widely applied wet filament winding on a rigid mandrel, which is considered in the present study. A schematic representation of this process is shown in Figure 2.

The manufacturing of fiber-reinforced polymer pipes involves winding reinforcing fibers onto a cylindrical mandrel. Glass or carbon fibers in the form of rovings are typically used as raw material. The rovings are fed from fiber spools through comb devices into a resin bath, where impregnation with resin occurs. Contact with an impregnation drum ensures uniform resin distribution within the fiber bundle. After leaving the resin bath, the impregnated fibers pass through comb devices and are supplied to the delivery head. After passing through the delivery head, the impregnated fiber bundle forms a tape of width h.

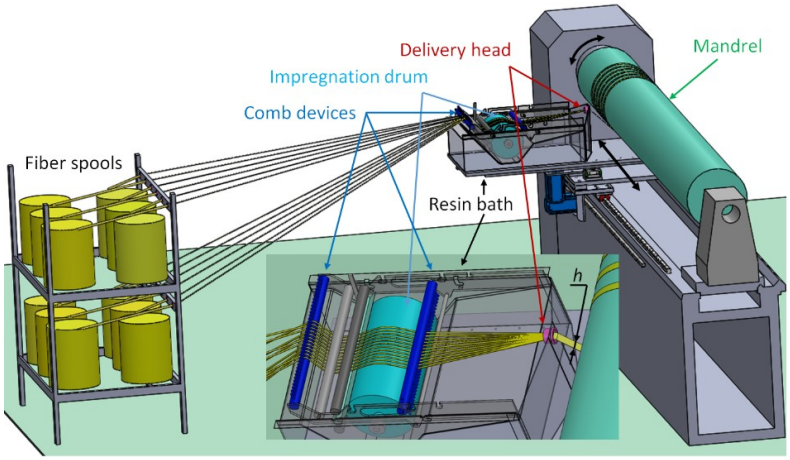

Figure 2: Scheme for production of pipes by winding on a cylindrical mandrel

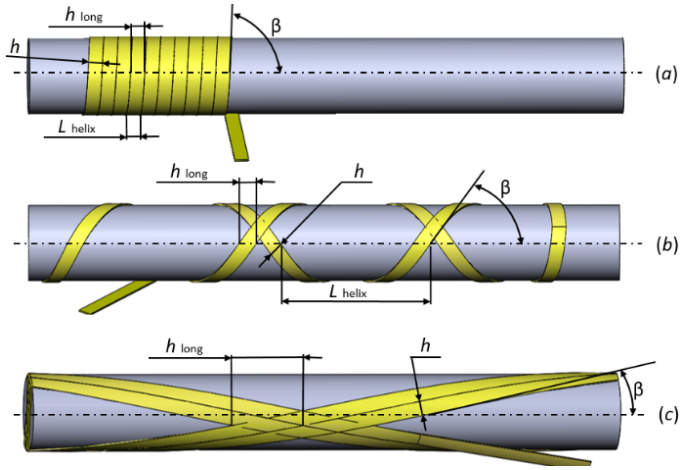

Figure 3: Schematic representation of three types of winding patterns: (a) is the circumferential winding; (b) and (c) are polar winding

This tape is wound onto the cylindrical mandrel, which rotates about its longitudinal axis, while the delivery head moves along the mandrel axis. The longitudinal motion of the delivery head defines the winding angle β, as illustrated in Figure 3.

The winding angle β determines the reinforcement scheme of the product and is selected according to the loading conditions and the required physical and mechanical properties of the pipe. Figure 3 presents basic winding pattern diagrams applicable to cylindrical fiber-reinforced shells. The winding angle β defines the orientation of reinforcing fibers relative to the longitudinal axis of the mandrel. In practice, winding is typically performed not with a single fiber, but with multiple fibers forming a tape of width h. Depending on the combination of tape width h and winding angle β, different winding patterns are obtained.

When the winding angle β approaches 90°, circumferential winding patterns are formed (Figure 3*a*). In circumferential winding, the winding angle is selected such that the winding pitch h_{helix} corresponds to the tape width along the mandrel axis h_{long}. Circumferential winding is commonly used to produce pipe sections with high circumferential stiffness or to create local transverse reinforcements.

In the range of winding angles β from 75° to 30°, helical winding patterns are formed. In helical winding, the winding pitch h_{helix} is chosen to be an integer multiple greater than the tape width along the mandrel axis h_{long}. In this case, multiple passes are required to fill the gaps between adjacent tapes and form a continuous layer. The winding angle for helical patterns is selected based on the loading conditions of the product and may be adjusted within a limited range to ensure uniformity of the pipe wall structure. Helical winding is widely applied in the manufacture of pipelines subjected to internal pressure.

At small winding angles β ranging from 30° to 0°, polar winding patterns are formed. The principle of layer formation in polar winding is similar to that of helical winding. Multiple passes are required to obtain a continuous layer. Polar winding is typically used for manufacturing components with high longitudinal stiffness operating under axial tension or compression.

In the present study, only helical and circumferential winding patterns are considered, as these methods are sufficient for the manufacture of pipelines intended for liquid transportation.

2.3 Models for Calculating Layer Parameters

When filament winding is performed on a rigid cylindrical mandrel, the pipe wall thickness is formed by the sequential addition of reinforcing layers. As a rule, each reinforcing layer is characterized by a specific fiber winding structure. Every layer must ensure uniform filling of its thickness with reinforcing fibers, without overlaps or gaps. Depending on the type of winding pattern, different models are applied to achieve uniform fiber distribution within the pipe wall. When developing a layer-filling model, the kinematic scheme of the winding machine must be taken into account. For winding pressure vessels, cones, or complex-shaped surfaces, four- or five-axis winding machines are typically used [4, 7, 22]. However, a pipe is a component bounded by a ruled cylindrical surface, and its manufacturing can be effectively carried out using a two-axis winding scheme. A schematic representation of such a machine is shown in Figure 4*b*. Its design includes one translational and one rotational motion. The orientation of the coordinate system relative to the machine depends on the machine configuration, and the axis directions follow the so-called right-hand “three-finger rule” in accordance with DIN 66217.

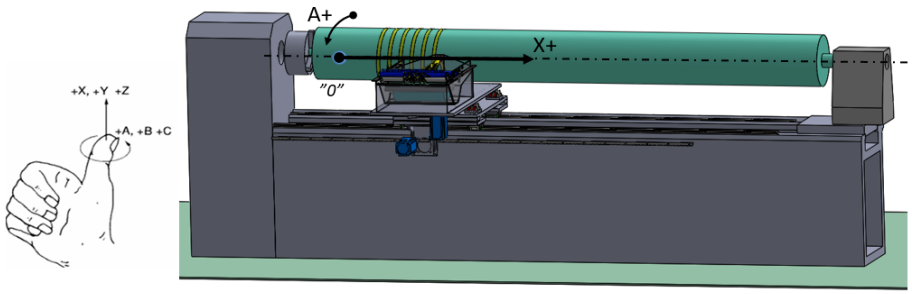

(a) (b)

Figure 4: Axis of movement in a 2-coordinate pipe winding scheme: (a) is the right-hand rule for selecting the direction of axes, (b) is the axis direction on an experimental winding machine

In the present study, the axis naming and directions commonly adopted as a standard in CNC systems are used (Figure 4*a*). The longitudinal movement of the delivery head along the mandrel axis corresponds to the X-axis, while the rotation of the mandrel about its longitudinal axis corresponds to the A-axis. Helical winding is the most widely used scheme for manufacturing pipes intended for the transportation of liquids and gases under pressure, as well as for tubular structural elements. The main mechanical characteristics of the pipe preform are determined by the reinforcement scheme, which is defined by the winding angle β [7, 9, 22]. In addition to the winding angle, the possibility of achieving uniform filling of the layer with reinforcing fibers also depends on the tape width h [22]. To fully fill a helical layer, it is generally necessary to perform multiple passes in two opposite directions. When changing the direction of motion along the mandrel axis, accurate positioning of the newly laid tape relative to the tape deposited during previous passes is required.

In the present study, a simple model for calculating the trajectories of the main and auxiliary passes of the delivery head is proposed.

The model is suitable for direct implementation within the CNC system of a winding machine.

The proposed approach ensures accurate positioning between successive passes and uniform filling of the reinforcing layer.

The implementation of a trajectory calculation model for circumferential winding complements the proposed approach to programming winding operations directly within the CNC system of the winding machine. Together, the developed models enable the creation of an integrated application that fully supports the manufacturing process of fiber-reinforced polymer pipes on a two-axis winding machine.

2.3.1 Helical Layer Model

The main parameters determining the winding trajectory and the relative motion of the mandrel and the delivery head are the mandrel diameter D, the winding angle β, and the tape width h (Figure 5).

The length of the mandrel surface covered by the tape during a single pass along the mandrel axis, h_{long}, is determined by the tape width h and the winding angle β as:

$$h_{long} = \frac{h}{\sin\left(\beta \cdot \frac{\pi}{180}\right)}. \quad (1)$$

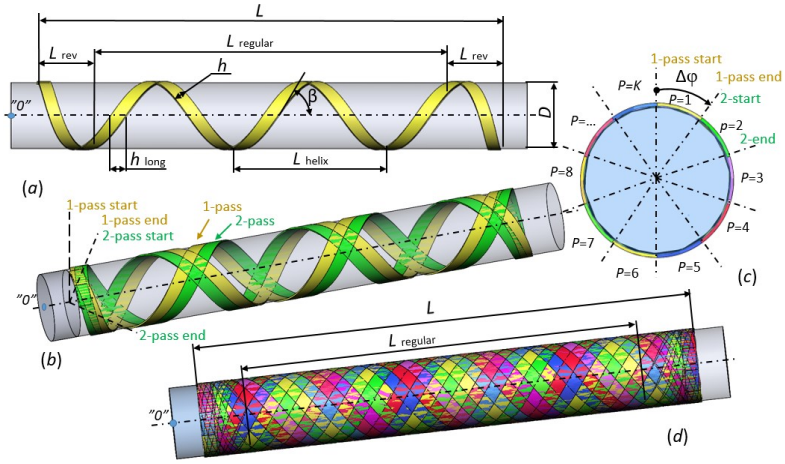

Figure 5: Schematic diagram of spiral winding in several passes: (a) is the main parameters of the winding pass; (b) is the mutual arrangement of two wind-ing passes; (c) is the diagram of uniform filling of the cross section with reinforcing fibers; (d) is the general view of the complete spiral winding layer

The winding pitch of the tape on the mandrel surface is defined as

$$L_{helix} = \frac{\pi \cdot D}{\tan\left(\beta \cdot \frac{\pi}{180}\right)}. \quad (2)$$

To ensure uniform filling of the winding layer, the tape must be laid on the mandrel surface without gaps or overlaps of rovings [22]. This condition can be satisfied when

$$L_{helix} = h_{long} \cdot K, \quad (3)$$

where K is the number of passes in one layer.

The number of passes K must be an integer. In practice, this condition is achieved by selecting the tape width h through variation of the number of rovings in the tape. As a result, the tape width cannot assume arbitrary values and changes discretely depending on the number of rovings. To satisfy condition (3), it is often necessary to adjust the winding angle β.

However, variations in β affect the physical and mechanical properties of the pipe wall material, and large deviations of the winding angle are unacceptable. Therefore, obtaining an acceptable combination of β and h represents a technological optimization problem that must be solved individually for each pipe.

In practice, this solution is not mathematically exact, and the degree of approximation to ideal surface coverage is characterized by the overlap coefficient

$$k_{overlap} = \frac{L_{helix}}{K \cdot h_{long}} = n \pm \Delta, \quad (4)$$

where n is an integer, and Δ represents the deviation from ideal surface coverage.

Ideal coverage corresponds to a single-layer arrangement of roving tapes without gaps or overlaps ($\Delta = 0$). Otherwise, the value of Δ indicates the fraction of the tape width by which adjacent passes overlap or leave gaps.

As shown in Figure 5*a* and Figure 5*d*, when winding a pipe of length L, each pass consists of a regular section ($L_{regular}$) and reversal sections (L_{rev}) at both ends. On the regular section, the winding angle β is strictly maintained, ensuring the desired mechanical properties of the pipe wall.

The reversal sections are technological zones in which, due to changes in fiber orientation, the mechanical properties differ from those of the regular section.

Uniform filling of the pipe wall thickness on the regular section can be achieved by shifting successive passes by an angular offset $\Delta\varphi$ (Figure 5*c*), defined as

$$\Delta\varphi = \frac{360^\circ}{K}. \quad (5)$$

With this offset, the edge of the tape in the subsequent pass comes into exact contact with the edge of the tape laid in the previous pass, ensuring uniform fiber distribution (Figure 5*b*). To achieve uniform filling, it is not mandatory to apply only consecutive offsets of $\Delta\varphi$. In some cases, offsets of $2 \cdot \Delta\varphi$, $3 \cdot \Delta\varphi$, or a predefined sequence of passes, for example $p = \{1, 4, 8, 2, \dots\}$, may be applied (Figure 5*c*).

Uniform filling of the reinforcing layer can also be ensured by shifting the starting point of each pass by the angular offset $\Delta\varphi$. One possible approach is rotating the mandrel to the starting position of the next pass ("2-start") after completing the first pass, regardless of the mandrel's angular position at the end of the previous pass (Figure 5*c*). However, this approach results in additional material accumulation at the pipe ends, leading to an unjustified increase in wall thickness.

In the present study, an alternative approach is proposed. The winding trajectory parameters are calculated so that the angular position of the mandrel at the end of each pass is always shifted relative to the starting position by $\Delta\varphi$. In this case, uniform filling of the reinforcing layer is achieved automatically by repeating the same winding trajectory K times, with each subsequent pass starting from the end point of the previous one.

Figure 6 shows the developed representation of a single winding pass trajectory in the *XA* coordinate system, corresponding to the kinematic scheme of the two-axis winding machine described above. The *X*-axis represents longitudinal movement along the mandrel axis, while the *A*-axis represents the angular position of the mandrel.

The total winding length L is defined as the difference between the start position P_s and the end position P_e of the delivery head. The reversal lengths L_{rev} near P_s and P_e are assumed to be equal. The displacement along the regular sections (points 1–2 and 4–5) is defined by L_{helix} and $\Delta r = 360°$.

The total angular displacement of the mandrel during one pass is given by

$$L_{rotary} = \varphi = N \cdot 360 + \Delta\varphi, \quad (6)$$

where N is the number of complete mandrel revolutions during one winding pass.

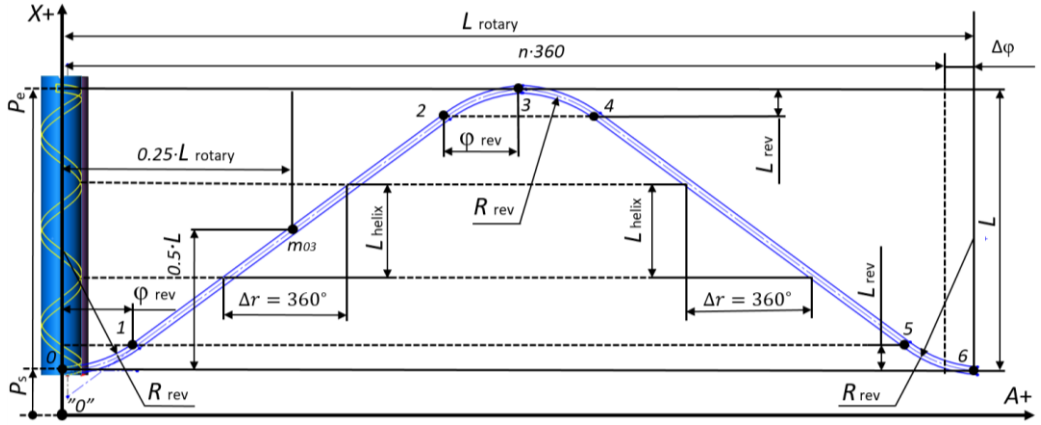

Figure 6: Scheme for determining the parameters of the trajectory of a single-pass helical winding

The value of N must satisfy

$$N \geq N_{calc} = \frac{2 \cdot L}{L_{helix}}. \tag{7}$$

To ensure high productivity of winding operations, the movements of the winding machine axes must be performed at high feed rates. In the reversal zones, this requires reversing the direction of motion of the longitudinal *X*-axis and changing the rotational speed of the *A*-axis. When winding trajectories are defined using linear interpolation, the CNC system inevitably generates deceleration zones at the ends of trajectory segments before changing the direction of motion. Such deceleration significantly reduces machine productivity. To enable continuous motion along the trajectory without unnecessary braking, smooth paths with a gradual change in the velocity vector direction must be applied [14]. These requirements can be satisfied by trajectories with conjugated circular arcs in the reversal zones, as shown in Figure 6. To determine the parameters of such trajectories, the coordinates of all nodal points must be calculated (Figure 6). The coordinates of points 0, 3, and 6 are known a priori, since the winding length L is specified as an input parameter and the value of L_{rotary} can be calculated using equation (6). In the zones of motion direction change of the delivery head, the coordinates of points 1, 2, 4, and 5 must be determined. For this purpose, it is necessary to calculate the axial displacement along the mandrel L_{rev}, the angular rotation of the mandrel φ_{rev}, and the radius of the conjugating arc R_{rev}.

To solve the problem of determining the trajectory parameters shown in Figure 6, a representative segment from point 0 to point m_{03} is considered. Point m_{03} represents the midpoint of the longitudinal displacement. Due to the symmetry of the selected trajectory, point m_{03} corresponds to one quarter of the rotational displacement of a single winding pass. The slope of the straight-line segment between points 1 and m_{03} is defined by the parameters L_{helix} and Δr. The center of the circular arc with radius R_{rev} lies on the *X*-axis, while point 1 represents the tangency point between the circular arc and the inclined straight-line segment. Simple geometric transformations make it possible to derive analytical expressions for calculating the required parameters of the circular trajectory segments in the motion reversal zones of the delivery head

$$\begin{aligned} R_{rev} &= \frac{-c}{a+\sqrt{a^2+b^2}}, \\ L_{rev} &= R_{rev} - R_{rev} \cdot \frac{\Delta r}{\sqrt{\Delta r^2 + L_{helix}{}^2}}, \\ \varphi_{rev} &= R_{rev} \cdot \frac{L_{helix}}{\sqrt{\Delta r^2 + L_{helix}{}^2}}, \end{aligned} \tag{8}$$

where $a = -\frac{1}{L_{helix}}$, $b = \frac{1}{\Delta r}$, $c = \frac{L}{2 \cdot L_{helix}} - \frac{L_{rotary}}{4 \cdot \Delta r}$.

Based on the proposed trajectory scheme and considering equation (7), the coordinates of points 1, 2, 4, and 5 can be calculated as

$$\begin{aligned} P_1 &= P_s + L_{rev}, & \varphi_1 &= \varphi_{rev}, \\ P_2 &= P_s + L - L_{rev}, & & \\ & & \varphi_2 &= 0.5 \cdot L_{rotary} - \varphi_{rev}, \\ P_4 &= P_s + L - L_{rev}, & & \\ & & \varphi_4 &= 0.5 \cdot L_{rotary} + \varphi_{rev}, \\ P_5 &= P_s + L_{rev}, & & \\ & & \varphi_5 &= L_{rotary} - \varphi_{rev}, \\ P_6 &= P_s, & \varphi_6 &= L_{rotary}. \end{aligned} \tag{9}$$

In these expressions, P_1, P_2, ... correspond to positioning coordinates along the longitudinal axis. In the CNC system considered in this study, parameter P corresponds to the *X*-axis, while φ_1, φ_2, ... correspond to the *A*-axis and define the angular displacement of the mandrel. A specific feature of the helical layer is that the completion of winding along the longitudinal *X*-axis always occurs at the starting position P_s of the winding section (Figure 6).

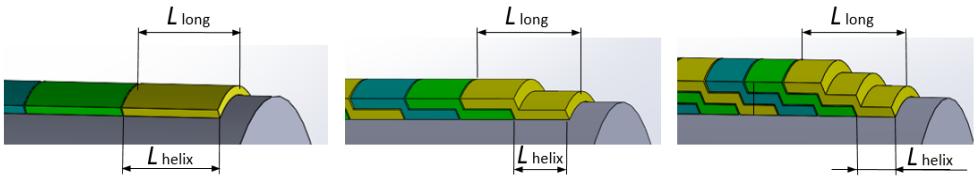

Figure 7: Formation of layer thickness by means of the overlap coefficient

2.3.2 Circumferential Winding Model

A specific feature of circumferential winding (Figure 3*a*) is that the layer is formed in a single pass. This means that the tape is wound at a winding angle β such that no gaps occur between adjacent turns. To obtain such a layer, the tape of width h must be wound onto a cylindrical mandrel of diameter D with a winding pitch L_{helix} not exceeding the tape width projected along the mandrel axis h_{long}. Therefore, the following condition must be satisfied:

$$L_{helix} \leq h_{long}. \tag{10}$$

The ratio of the tape width along the mandrel axis h_{long} to the winding pitch L_{helix} defines the overlap coefficient

$$k_{overlap} = \frac{h_{long}}{L_{helix}}. \tag{11}$$

During circumferential winding, the layer thickness can be controlled by varying the overlap coefficient $k_{overlap}$. Figure 7 illustrates different options for forming layer thickness using the overlap coefficient. When $k_{overlap} = 1$, a layer with thickness δ equal to the tape thickness is formed (Figure 7*a*). When the winding pitch is set to L_{helix}=0.5h_{long}, the overlap coefficient becomes $k_{overlap} = 2$, and the resulting layer thickness equals $2 \cdot \delta$ (Figure 7*b*). Accordingly, at $k_{overlap} = 3$, a layer with thickness $3 \cdot \delta$ is formed (Figure 7*c*).

In Figure 7, integer values of the overlap coefficient are shown, which are typically applied to ensure uniform filling of the wall thickness with reinforcing material, as is characteristic for winding with woven tapes. When winding with rovings, reinforcing fibers are distributed more evenly across the wall thickness; therefore, the use of non-integer values of the overlap coefficient is permissible. However, in this case, the formation of a wall with non-uniform thickness may occur.

The minimum thickness of a circumferential layer, equal to the tape thickness, is obtained when $k_{overlap} = 1$. This condition is satisfying when winding is performed at the angle $\beta = \beta_{calc}$, which is determined by

$$\beta_{calc} = 90 - arcsin\left(\frac{h}{\pi \cdot D}\right) \cdot \frac{180}{\pi}. \tag{12}$$

Figure 8 shows the scheme for constructing the developed trajectory representation for circumferential winding. When winding along the trajectory segment 1–2 at the winding angle $\beta = \beta_{calc}$, a circumferential layer with thickness equal to the tape thickness is formed. The longitudinal displacement step h_{long} is defined by equation (1). The angular displacement of the mandrel around its axis along this regular section of the circumferential layer is given by

$$\varphi_{reg} = 360° \cdot \left(L/L_{helix}\right). \tag{13}$$

Certain features of circumferential winding should be noted. As shown in Figure 9*a*, due to the helical arrangement of the tape during circumferential winding, complete filling of the reinforcing layer is not achieved at the initial cross section. To eliminate this defect, winding must be performed without longitudinal movement of the delivery head over an initial angular displacement φ_s before starting the helical motion. A similar issue arises at the end cross section of the circumferential layer when point 2 is reached (Figure 8). To fill the end cross section, winding without longitudinal movement of the delivery head is performed over an angular displacement φ_e (Figure 9*b*).

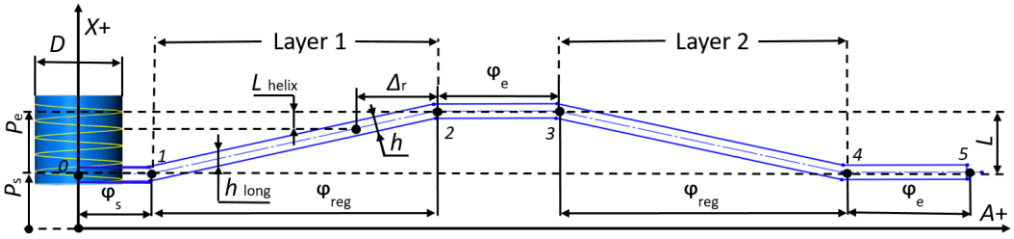

Figure 8: Scheme for determining the parameters of the trajectory for circumferential winding

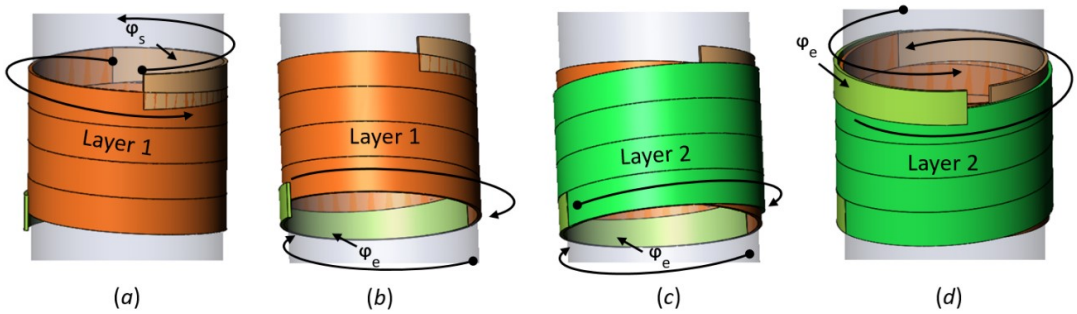

Figure 9: Winding sections without longitudinal movement of the delivery head

Thus, winding of a single circumferential layer starts at the initial point P_s and ends at the final point P_e. In the general case, winding of a single circumferential layer consists of three stages:

- winding without longitudinal movement of the delivery head over the angle φ_s at the initial cross section;
- helical winding with longitudinal step h_{long} while moving from P_s to P_e;
- winding without longitudinal movement of the delivery head over the angle φ_e at the final cross section.

In many cases, circumferential winding is required to form a layer with a thickness equal to several tape thicknesses. This can be achieved by performing multiple winding passes in forward and reverse directions within the interval between points P_s and P_e (Figure 8). The figure shows a developed trajectory for an even number of passes, corresponding to winding two layers. Layer 1 is wounded while moving from P_s to P_e, whereas Layer 2 is wound in the opposite direction from P_e to P_s. Winding of an even number of layers is completed at the initial point P_s. It should be noted that only the first layer consists of three motion stages. The second and all subsequent layers are formed using two motions only: helical winding with step h_{long} and winding without longitudinal movement of the delivery head during layer completion by rotating the mandrel through the angle φ_e (Figure 9*c*, *d*).

According to the proposed trajectory scheme (Figure 8) and the winding procedure described above, the coordinates of points 1, 2, 3, 4, and 5 for circumferential winding can be calculated as

$$\begin{aligned} P_1 &= P_s, & \varphi_1 &= \varphi_s, \\ P_2 &= P_s + L = P_e, & \varphi_2 &= \varphi_s + \varphi_{reg}, \\ P_3 &= P_e, & & \\ & & \varphi_3 &= \varphi_s + \varphi_{reg} + \varphi_e, \\ P_4 &= P_s, & & \\ & & \varphi_4 &= \varphi_s + 2 \cdot \varphi_{reg} + \varphi_e, \\ P_5 &= P_s, & & \\ & & \varphi_5 &= \varphi_s + 2 \cdot \varphi_{reg} + 2 \cdot \varphi_e. \end{aligned} \quad (14)$$

As in equation (8), the values P_1, P_2, … correspond to the positioning coordinate along the longitudinal *X*-axis, while the parameters φ_1, φ_2, … correspond to the *A*-axis and define the angular displacement of the mandrel about its axis.

2.3.3 Model of Transitions Between Layers

The structure of a fiber-reinforced polymer pipe typically consists of several layers of different types. Consideration of operating conditions, installation features, and joint configurations may require the formation of a structure in which multiple layers with different lengths and different axial positions along the pipe are wound (Figure 10). This, in turn, necessitates performing a transition from the end point of the previously wound layer $Layer(i-1)$ to the starting point of the subsequent layer $Layer(i)$.

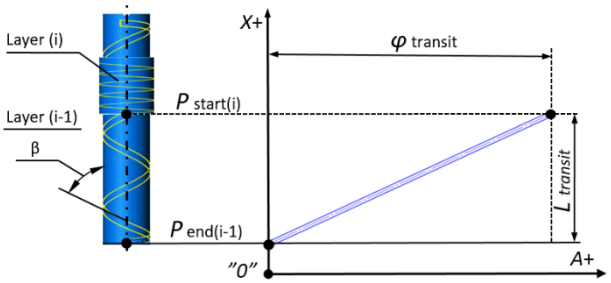

Figure 10: Scheme for calculating transition parameters between layers

Such a transition requires axial movement along the mandrel by a distance

$$L_{transit} = P_{start}(i) - P_{end}(i-1). \quad (15)$$

A natural and technologically justified solution is to perform this transition along a helical trajectory, defined by a selected transition winding angle β. In this case, the mandrel must rotate through an angle

$$\varphi_{transit} = \frac{L_{transit}}{D} \cdot tg\left(\beta \cdot \frac{\pi}{180}\right) \cdot 360. \quad (16)$$

During the transition, it may be necessary to fix the tape at the reached axial position. In the proposed model, this requirement is satisfied by performing circumferential winding through a

specified angular displacement φ_s (Figure 8), which is applied at the beginning of each subsequent layer.

3. Integration of Interactive Programming Procedures into the CNC System

3.1 Context Model of the Winding Process

To formalize the filament winding process, a comprehensive set of models was developed to represent the execution sequence, as well as the resource and information support of the process. Process modeling was carried out using the IDEF0 and IDEF3 notations in the specialized process modeling software AllFusion Process Modeler.

For process analysis, the IDEF0 notation was applied, as it enables the identification and description of system or process functions and their interrelationships. The context diagram shown in Figure 11 provides a generalized description of the winding parameter calculation process. The input data includes the mandrel diameter, winding angle, winding length, tape width, and permissible tape overlap. Process control is performed in accordance with constraints inherent to automated manufacturing and the calculation methodology implementing the mathematical model of pipe layer winding. The output of the process consists of calculation results that enable the generation of winding trajectories for CNC-controlled equipment.

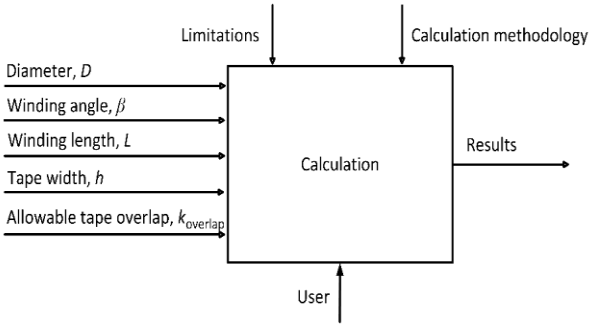

Figure 11: Context model of the winding process

As a result of decomposing the context model, a process decomposition diagram was developed (Figure 12), illustrating the execution sequence and interaction of process elements while accounting for input parameters such as mandrel diameter, winding angle, tape width, and the winding section length defined as the longitudinal positioning interval between the initial position P_s and the final position P_e of the delivery head. The permissible overlap of the roving tape is evaluated through constraints on the deviation of the overlap coefficient $k_{overlap}$ from an integer value. The model incorporates technical and technological constraints implemented in the information-processing algorithms at the corresponding stages of the process design procedure.

At the first stage, a preliminary determination of the winding pitch per mandrel revolution L_{helix} is performed based on the specified mandrel diameter D and the desired winding angle β, in accordance with the selected calculation methodology. The output of block A1 is the preliminary value of the winding pitch. This information, together with the tape width h and the longitudinal winding interval (P_s, P_e), is used to calculate the parameters of the helical winding pass that ensures coverage of the mandrel surface. The output of block A2 is the tape width projected along the mandrel axis, h_{long}.

As a result of recalculating the winding angle in block A3, the actual value of the winding angle is determined and subsequently used in block A4 to calculate the total mandrel rotation angle per pass, L_{rotary}. Based on these results, block A5 determines the tape overlap coefficient $k_{overlap}$, which characterizes the uniformity of wall thickness formation. Following the preliminary calculations, the execution of blocks A2–A5 is performed iteratively to obtain an acceptable value of the overlap coefficient $k_{overlap}$. The calculation of winding trajectory point coordinates is carried out in block A6.

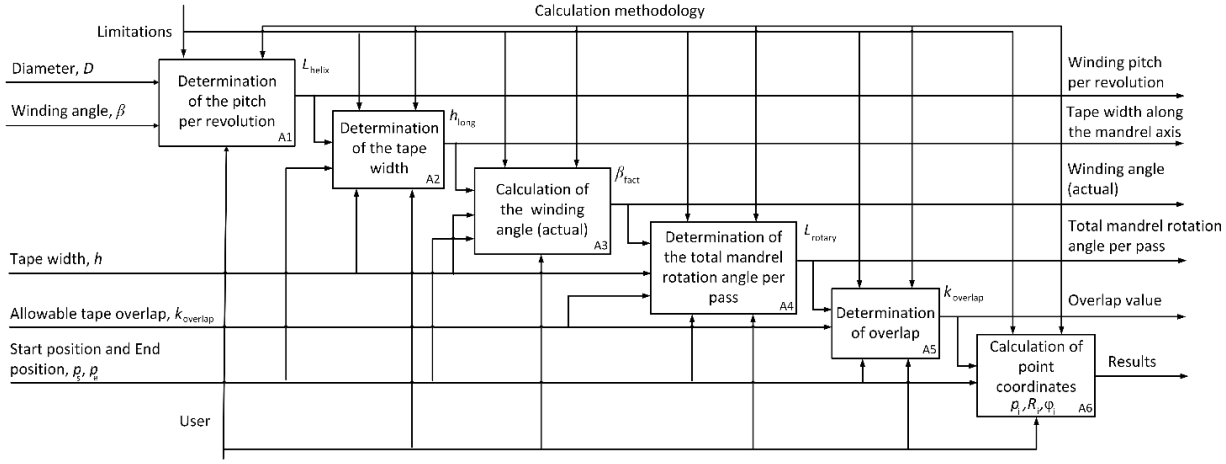

Figure 12: Process decomposition model (IDEF0)

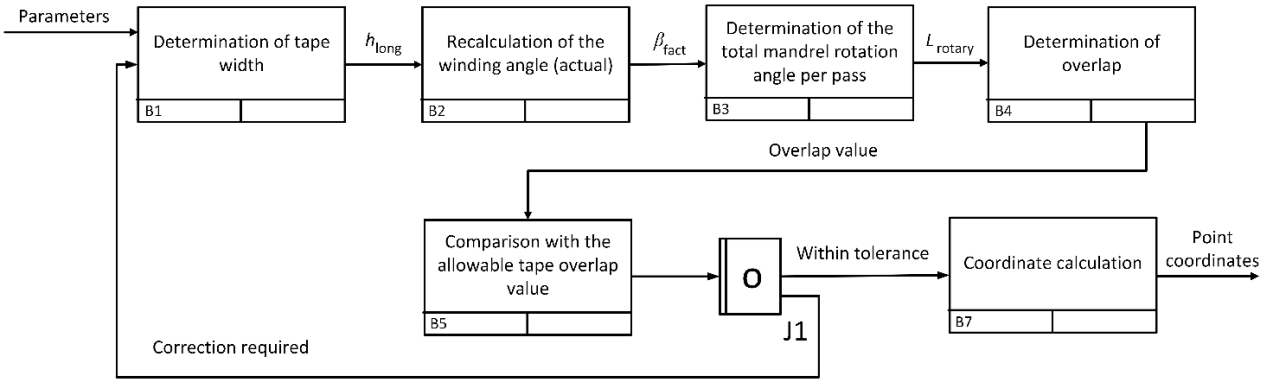

Figure 13: IDEF3 model of the winding process

To formalize the topology of the iterative part of the process, a model in the IDEF3 format was developed (Figure 13). At the initial stage, based on the specified input parameters, the tape width projected along the mandrel axis h_{long} is determined (block B1). This is followed by recalculation of the winding angle β (block B2) considering the actual geometric conditions. Subsequently, the corrected winding angle is used to calculate the total mandrel rotation angle per pass L_{rotary} (block B3). The final stage of the main linear branch is the determination of the overlap value (block B4), which characterizes the degree of pass overlap within a single winding layer.

The obtained overlap value is then passed to the comparison block B5, after which the verification result is transferred to the logical node J1, which implements an XOR branching (type "0") in the IDEF3 model and ensures selection of one of the alternative execution scenarios. If the overlap value falls within the specified permissible limits, the process proceeds through node J1 to the coordinate calculation block B7, which generates the output data. If the admissibility condition is not satisfied, the algorithm returns to the previous stages, providing iterative recalculation of the winding angle and correction of geometric variables until the specified criteria are achieved.

3.2 Models Implementation in CNC Software

The developed models were implemented and experimentally validated on equipment equipped with a two-level CNC system [15, 23]. The interactive software for designing the filament winding process of pipelines was integrated into the CNC program code editing subsystem at the upper level of the two-level CNC architecture.

The software was developed as an MFC application in the Visual Studio 15 environment. Figure 14 shows the main window for designing the structure of winding pipe layers. The window is divided into four functional areas.

The first area (Figure 14, p. 1) displays the structural configuration of the layers designed for winding a specific pipe. The ability to alternate helical layers with different winding angles and circumferential layers with different axial positions along the mandrel allows the formation of pipes with complex reinforcement schemes and local strengthening zones.

The second area (Figure 14, p. 2) contains the layer management panel, which provides tools for creating, reordering, editing, and deleting winding layers.

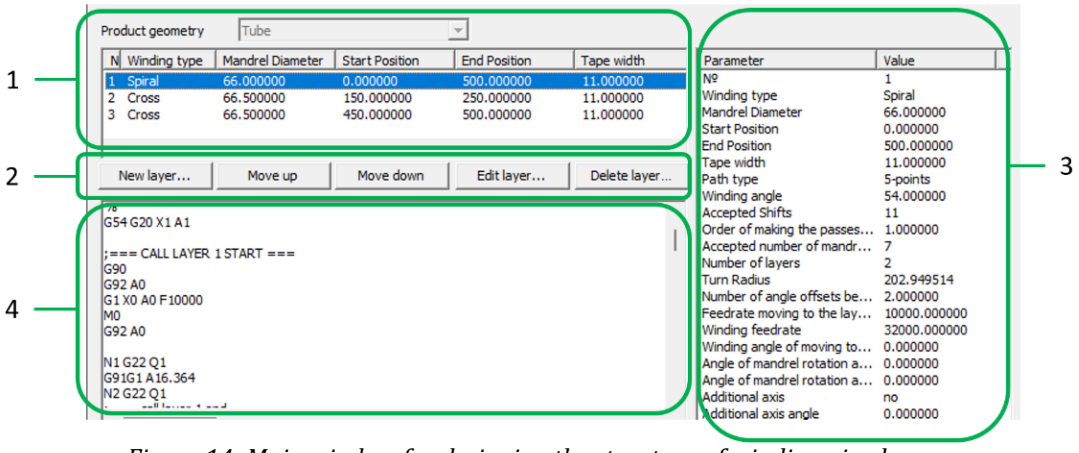

Figure 14: Main window for designing the structure of winding pipe layers

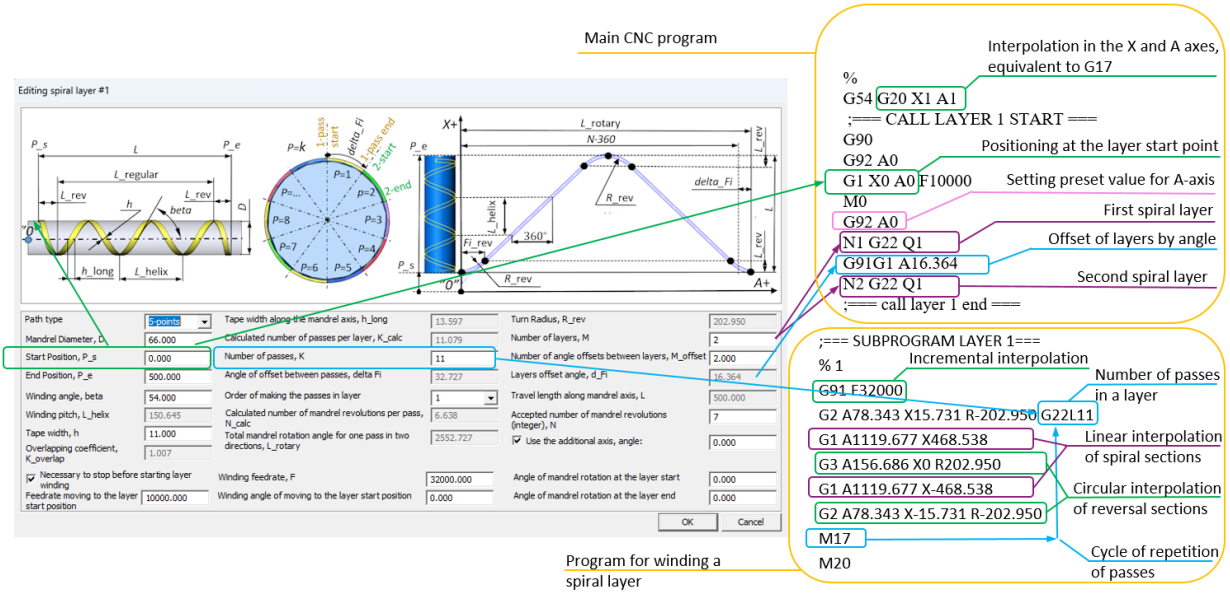

Figure 15: Dialog box for designing a helical winding layer and the corresponding CNC winding code

The third area (Figure 14, p. 3) displays the parameters of the layer selected in area 1, while the fourth area shows the CNC code of the designed winding program. In this window, only the layer structure can be modified, whereas winding parameters and CNC code are displayed in read-only mode.

The design of a helical winding layer is performed through interactive interaction with a dedicated dialog window (Figure 15). In accordance with the IDEF0 scheme (Figure 12), the operator inputs the initial data, after which the system performs the calculations and displays the parameters of a feasible solution. In addition to the main input parameters, the operator can adjust several key variables, including the accepted number of passes K (Eq. 3), the accepted number of mandrel rotations N (Eq. 7), and the order of passes within a layer.

Figure 15 presents an example of designing a helical winding program for a pipe with an inner diameter $D = 66$ mm, a winding length of 500 mm, a roving tape width $h = 11$ mm, and a fiber winding angle $\beta = 54°$.

CNC code generation is performed automatically after confirmation of the input data. Figure 15 shows the CNC program code generated for the test pipe. The winding trajectory code of the layer is implemented as a subprogram (%1). The base pass, according to the scheme shown in Figure 6, consists of five blocks: two G1 commands defining linear interpolation of the spiral sections and three G2/G3 commands defining circular interpolation of the reversal sections. The number of passes in a layer determines how many times the pass is repeated to form complete layer coverage. The pass repetition cycle is programmed using the G22 and M17 commands, with the number of repetitions specified by address L.

The main CNC program (Figure 15) defines the general execution conditions and performs calls to the layer winding subprograms. The G20 X1 A1 function is used to define the interpolation plane in the X and A axes. This function is equivalent to G17 and enables circular interpolation for arbitrary combinations of axes. In the presented example, winding of two identical layers is specified by the parameter "Number of layers" M = 2. The winding procedure for the corresponding layers is invoked using the G22 Q1 command, where address Q specifies the number of the layer winding subprogram. Between successive layer calls, an incremental angular offset between layers is applied to shift the lateral edges of the tapes relative to each other, ensuring uniform filling of the wall thickness with reinforcing fibers.

The programming of circumferential layers is implemented in a similar manner. The winding procedure of a layer is defined in a dedicated subprogram. In the main CNC program, positioning at the layer start point is performed (e.g., G1 X450 …), followed by a call to the corresponding layer winding procedure (N4 G22 Q3). In the example shown in Figure 16, subprogram (%3) corresponds to winding Layer No. 3 within the longitudinal positioning interval from $P_s = 450$ mm to $P_e = 500$ mm.

In this case, the winding pitch L_{helix} is equal to half of the tape width h, resulting in an overlap coefficient $k_{overlap} = 2.003$. As a result, wall thickness equal to two tape thicknesses is formed in a single pass. At the beginning of layer winding, mandrel rotation by the angle $\varphi_{start} = 210°$ is programmed in accordance with the layer start formation scheme (Figure 16*a*).

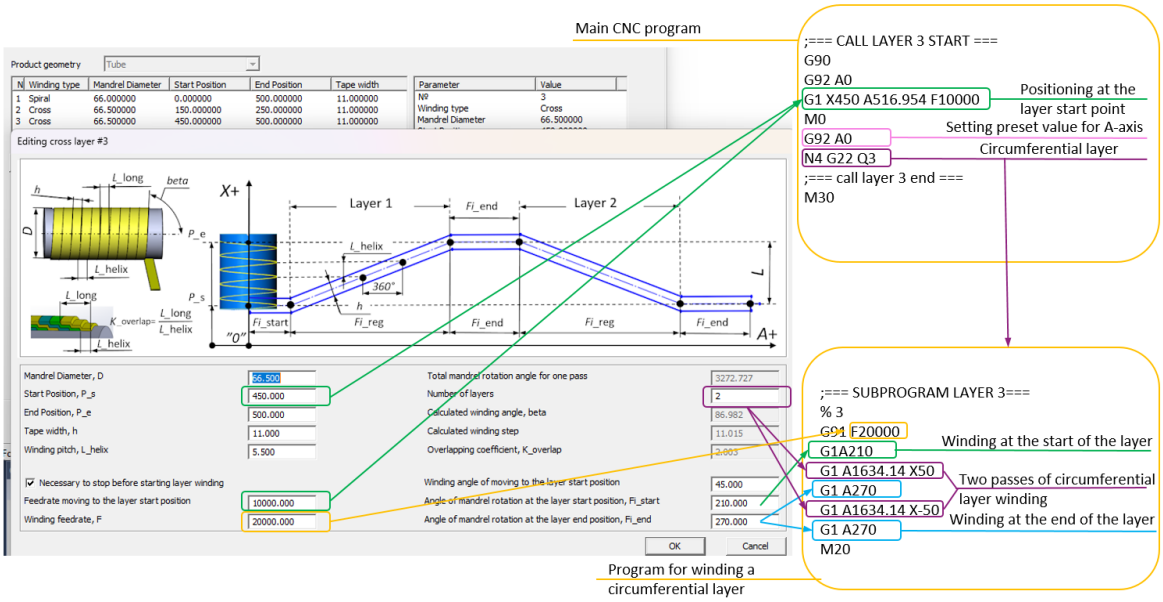

Figure 16: Dialog box for designing a circumferential winding layer and the corresponding CNC winding code

4. Experimental Validation on CNC Equipment

Experimental validation of the interactive programming application was carried out on a two-axis winding machine. The tests were performed using a pipe specimen with an inner diameter of 66 mm and a winding length of 500 mm, intended – after minor modification – for use as a structural element of a cryogenic device [24].

An example of the winding program used for the experiments was presented in the previous sections. Winding was performed using glass-fiber roving. The tape width was $h = 11$ mm, and the winding angle was set to $\beta = 54°$.

According to the winding program (Figure 15), formation of a complete helical layer required 11 passes. Figure 17*a* shows the state of the specimen after completion of the first winding pass, while Figure 17*b* illustrates the completion of the eleventh pass and the formation of a full helical layer.

In accordance with the test program, two helical layers were wound. The winding of a local thickening formed by a circumferential layer was performed in compliance with the program shown in Figure 16. The process of winding the local thickening is shown in Figure 17*c*, while the finished pipe specimen after polymerization is shown in Figure 17*d*.

The wall thickness of the pipe in the helical winding region was measured to be 1.1 mm, with a maximum deviation not exceeding ±0.1 mm.

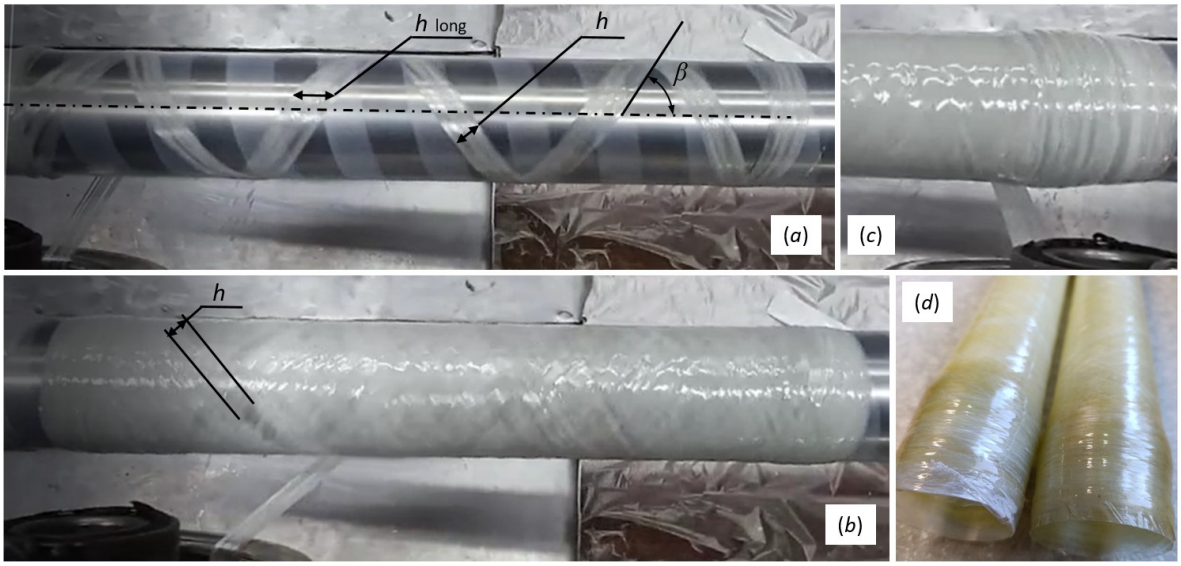

Figure 17: Experimental validation of the filament winding process: (a) is the completion of the first winding pass; (b) is the completion of the eleventh pass and formation of a full helical layer; (c) is the winding of a local circumferential thickening; (d) is the finished pipe specimen after polymerization

This result indicates stable process execution and uniform filling of the layer with reinforcing fibers, demonstrating the practical applicability of the proposed interactive CNC-based programming approach.

5. Conclusions

This study proposed and validated an approach to interactive programming of filament winding operations implemented directly within CNC systems of low-cost two-axis winding machines, without reliance on external CAM software. The approach is based on analytical models for helical and circumferential winding layers, as well as transition trajectories between layers, and is oriented toward practical use in the manufacturing of fiber-reinforced polymer pipelines.

The developed mathematical models enable accurate generation of winding trajectories with controlled overlaps and uniform distribution of reinforcing fibers within the pipe wall. A distinctive feature of the proposed methodology is the use of circular interpolation in motion reversal zones, which ensures smooth variation of velocity and acceleration and eliminates unnecessary braking, which is expected to contribute to stable process operation during winding. The inclusion of dedicated models for interlayer transitions makes it possible to form multilayer pipe structures with different axial extents and local reinforcements along the pipe length.

The proposed models were successfully implemented in an interactive CNC software application integrated into the upper level of a two-level CNC system. The developed software supports layer-by-layer design of winding structures, automatic calculation of winding parameters, and direct generation of CNC programs, significantly reducing the complexity of process preparation and increasing its transparency for the operator.

Experimental validation carried out on a low-cost two-axis winding machine confirmed stable execution of the programmed trajectories and regular winding patterns. The measured wall thickness deviation in the helical winding region did not exceed ±0.1 mm, demonstrating uniform filling of the reinforcing layer and validating the adequacy of the proposed models and programming approach.

The obtained results demonstrate that interactive CNC-based programming represents an effective and practical alternative to traditional CAM-based solutions for filament winding of cylindrical pipelines, particularly for low-cost equipment with a limited number of controlled axes. Further development of the proposed approach will focus on its extension to multi-axis winding systems, integration of adaptive control strategies based on process feedback, and coupling with predictive models of mechanical properties for automated optimization of winding structures.

Acknowledgement

The study was supported by the Ministry of Education and Science of Ukraine as part of scientific research project No. 0125U001021.

References

[1] Kennedy, S.M., Robert, R.J., Prince, R.M.R., Hikku, G.S., & Kaliraj, M. (2024). A comprehensive overview of the fabrication and testing methods of FRP composite pipes. *MethodsX, 13*, 102990. https://doi.org/10.1016/j.mex.2024.102990

[2] Alabtah, F.G., Mahdi, E., & Eliyan, F.F. (2021). The use of fiber reinforced polymeric composites in pipelines: A review. *Composite Structures, 276*, 114595. https://doi.org/10.1016/j.compstruct.2021.114595

[3] Kivirenko, O., Kostenko, S., Sorokin, V., Tsegelnyk, Y., Plankovskyy, S., & Kombarov, V. (2023). Fiberglass pipeline continuous filament winding automation. *International Journal of Mechatronics and Applied Mechanics, 2023*(14), 241–247. https://doi.org/10.17683/ijomam/issue14.28

[4] Man, R., Ma, Z., Yin, Z., Ye, L., & Ma, W. (2025). Filament winding pattern generation for non-axisymmetric mandrels based on path adaptive adjustment. *Journal of Composite Materials, 59*(5), 699–709. https://doi.org/10.1177/00219983241300146

[5] Lyakhno, V.Y., Fedorchenko, A.V., Kivirenko, O.B., & Shnyrkov, V.I. (2009). FRP Dewar for measurements in high pulsed magnetic fields. *Cryogenics, 49*(8), 425–428. https://doi.org/10.1016/j.cryogenics.2009.06.004

[6] Kharouf, N., Sauro, S., Hardan, L., Jmal, H., Bachagha, G., Macaluso, V., ... & Mancino, D. (2022). Compressive strength and porosity evaluation of innovative bidirectional spiral winding fiber reinforced composites. *Journal of Clinical Medicine, 11*(22), 6754. https://doi.org/10.3390/jcm11226754

[7] Chen, C.L., Chen, L.H., & Yau, H.T. (2023). Winding pattern planning and control of a filament winding machine for gas-cylinders. *Machines, 11*(6), 635. https://doi.org/10.3390/machines11060635

[8] Quanjin, M., Rejab, M.R.M., Kaige, J., Idris, M.S., & Harith, M.N. (2018). Filament winding technique, experiment and simulation analysis on tubular structure. *IOP Conference Series: Materials Science and Engineering, 342*, 012029. https://doi.org/10.1088/1757-899X/342/1/012029

[9] Saif, T., Saad, N., Al-Zubiedy, A., & Idzikowski, A. (2022). Effect of ply angle on the burst pressure of composite pressure vessels by filament winding. *Construction of Optimized Energy*

Potential, 11, 223–233. https://doi.org/10.17512/bozpe.2022.11.25

[10] Andrianov, A., Tomita, E.K., Veras, C.A.G., & Telles, B. (2022). A low-cost filament winding technology for university laboratories and startups. *Polymers, 14*(5), 1066. https://doi.org/10.3390/polym14051066

[11] Hashim, M.F.A., Ghazali, C.M.R., Daud, Y.M., Zainal, F.F., Faris, M.A., Si, H.M., ... & Razani, M.S.M. (2020). Effect of winding speed in epoxy glass composites for new fabricated filament winding machine. *AIP Conference Proceedings, 2291*, 020034. https://doi.org/10.1063/5.0023502

[12] Rojas, E.V., Chapelle, D., Perreux, D., Delobelle, B., & Thiebaud, F. (2014). Unified approach of filament winding applied to complex shape mandrels. *Composite Structures, 116*, 805–813. https://doi.org/10.1016/j.compstruct.2014.06.009

[13] Xu, Y., Mohd Zaman, M.H., & Zhou, F. (2026). Optimized continuous small line interpolation algorithm for high end CNC machine tools using a cross segment approach. *Scientific Reports, 16*, 1133. https://doi.org/10.1038/s41598-025-30782-z

[14] Kombarov, V., Fojtu, P., Sulitka, M., Aksonov, Y., Sveda, J., Tsegelnyk, Y., ... & Plankovskyy, S. (2025). Prediction and compensation of motion differential characteristics influence on position error in CNC machine tools. *The International Journal of Advanced Manufacturing Technology, 137*(11), 5951–5981. https://doi.org/10.1007/s00170-025-15510-1

[15] Kombarov, V., Sorokin, V., Tsegelnyk, Y., Plankovskyy, S., & Aksonov, Y. (2023). S-shape feedrate profile with smoothly-limited jerk for threading movements synchronization in CNC machining. In O. Arsenyeva, T. Romanova, M. Sukhonos, Y. Tsegelnyk (Eds.) *Smart Technologies in Urban Engineering*. LNNS, vol. 536 (pp. 593–605). Springer. https://doi.org/10.1007/978-3-031-20141-7_54

[16] Gaidachuk, O., Kondratiev, A., Taranenko, I., Nabokina, T., & Zaverukha, V. (2023). Method of winding of small-diameter pipes using vibration effects. In O. Arsenyeva, T. Romanova, M. Sukhonos, I. Biletskyi, Y. Tsegelnyk (Eds.) *Smart Technologies in Urban Engineering*. LNNS, vol. 807 (pp. 175–184). Springer. https://doi.org/10.1007/978-3-031-46874-2_16

[17] Sokolovskyi, M., & Bernatskyi, A. (2023). Developmental review of metal additive manufacturing processes. *History of Science and Technology, 13*(2), 334–356. https://doi.org/10.32703/2415-7422-2023-13-2-334-356

[18] Dobrotvorskiy, S., Dobrovolska, L., Basova, Y., & Aleksenko, B. (2019). Particulars of adsorbent regeneration with the use of microwave energy. *Acta Polytechnica, 59*(1), 12–23. https://doi.org/10.14311/AP.2019.59.0012

[19] Pliuhin, V., Plankovskyy, S., Zablodskiy, M., Biletskyi, I., Tsegelnyk, Y., Kombarov, V. (2023). Novel features of special purpose induction electrical machines object-oriented design. In D.D. Cioboată (Eds.) *International Conference on Reliable Systems Engineering (ICoRSE) – 2022*. LNNS, vol. 534 (pp. 265–283). Springer. https://doi.org/10.1007/978-3-031-15944-2_25

[20] Quanjin, M., Rejab, M., Sahat, I., Amiruddin, M., Bachtiar, D., Siregar, J.P., & Ibrahim, M.I. (2018). Design of portable 3-axis filament winding machine with inexpensive control system. *Journal of Mechanical Engineering and Sciences, 12*(1), 3479–3493. https://doi.org/10.15282/jmes.12.1.2018.15.0309

[21] Gao, Q., Wang, W., & Lou, K. (2024). Research on innovative mechanical structure design in carbon fiber ingot winding technology. *Applied Mathematics and Nonlinear Sciences, 9*(1), 1–22. https://doi.org/10.2478/amns-2024-2606

[22] Mlýnek, J., Petrů, M., Ryvolova, M., & Rahimian Koloor, S.S. (2022). Winding optimization of composite frame by dry fiber rovings. *Journal of Industrial Textiles, 52*, 15280837221114639. https://doi.org/10.1177/15280837221114639

[23] Tsegelnyk, Y., Kombarov, V., Plankovskyy, S., Aksonov, Y., Pliuhin, V., & Aksonov, O. (2022). Investigation of the portal-type machine tool gear-belt gearbox. *International Journal of Mechatronics and Applied Mechanics, 2022*(11), 295–302. https://doi.org/10.17683/ijomam/issue11.41

[24] Budnyk, M.M., Minov, Y.D., Lyakhno, V.Y., Desnenko, V.A., Linnik, A.S., & Shopen, O.B. (2018). Development of improved superconductive axial gradiometers for biomagnetic SQUID applications. *Low Temperature Physics, 44*(3), 233–237. https://doi.org/10.1063/1.5024543